Journal of
Marine Science and Engineering

MDPI

Article

Effect of Rigid Vegetation Arrangement on the Mixed Layer of Curved Channel Flow

Tianwei Huang [1], Mengxing He [1], Kan Hong [2], Yingtien Lin [1,3,4,*] and Pengcheng Jiao [1,3,4,*]

1 Institute of Port, Coastal and Offshore Engineering, Ocean College, Zhejiang University, Zhoushan 316021, China
2 Liangshi Technology Ltd., Hangzhou 310009, China
3 Engineering Research Center of Oceanic Sensing Technology and Equipment, Zhejiang University, Ministry of Education, Zhoushan 316021, China
4 Donghai Laboratory, Zhoushan 316021, China
* Correspondence: kevinlin@zju.edu.cn (Y.-T.L.); pjiao@zju.edu.cn (P.J.)

Abstract: Curved channels and aquatic vegetation are commonly present in the riverine environment. In this study, the effects of vegetation density and distribution on the hydrodynamic characteristics of a mixed layer developed over a 180-degree curved channel were investigated through flume experiments. Wooden sticks were used to simulate rigid vegetation distributed along the half side of the channel, and a 200 Hz acoustic Doppler velocimeter (ADV) was employed to measure the three-dimensional instantaneous velocity at five selected cross sections along the curved channel. Experimental results show that the vegetation covering the half of the channel significantly affects the hydrodynamic structure of the curved channel flow, and the unequal vegetation resistance induces the K-H instability at the vegetation and non-vegetation interface, resulting in a standard hyperbolic tangent function of streamwise velocity distribution along the lateral direction. The influence of curve position on turbulence kinetic energy is far greater than that of vegetation density and vegetation distribution. The peak value of turbulent kinetic energy is comprehensively affected by vegetation density and distribution, and the peak position of turbulent kinetic energy at the interface is changed by different vegetation distribution. The combined effect of the curve and the partly covered vegetation increases the mixing between the water bodies, enhancing turbulent kinetic energy, and vegetation along the concave bank plays a more significant role. For turbulent bursting, the inward and outward interactions are mainly bursting events in the vegetation area, while ejections and sweeps are dominant in the non-vegetation area. However, the critical vegetation condition to initiate large-scale coherent structure (LSS) in the mixed layer and the influence of flexible vegetation need to be further studied in the future.

Keywords: emerged rigid vegetation; curved channel; mixed layer; turbulent kinetic energy; power spectral analysis

check for updates

Citation: Huang, T.; He, M.; Hong, K.; Lin, Y.; Jiao, P. Effect of Rigid Vegetation Arrangement on the Mixed Layer of Curved Channel Flow. *J. Mar. Sci. Eng.* **2023**, *11*, 213. https://doi.org/10.3390/jmse11010213

Academic Editors: Yuriy Semenov, Alexander Korobkin and Baoyu Ni

Received: 27 November 2022
Revised: 8 January 2023
Accepted: 11 January 2023
Published: 13 January 2023

1. Introduction

Flow in an open curved channel is commonly observed in nature and hydraulic engineering. Due to the existence of the centrifugal force in the bend, the flow forms a spiral movement (main circulation) along the cross section of the bend [1]. The spiral movement will lead to the uneven distribution of flow velocity, erosion and sedimentation of the bank, and the diffusion of sediment and pollutants [2]. In recent years, experiments have also found that there is a secondary circulation in the area near the water surface at the concave bank of the bend opposite to the rotation direction of the main circulation, which plays an important role to protect on the concave bank of the river from erosion [3,4]. Therefore, it is of great practical value to study the turbulent characteristics of bend flow for river regulation, water diversion works, channel navigation, etc. Because of the complexity of the turbulent mechanism of the bend flow, most of the actual flow problems cannot be solved analytically. In addition, it requires a lot of logistical efforts to carry out field measurement in natural rivers, so laboratory experiments are favorable alternatives to study the turbulence characteristics of flow in a curved channel. In the 1950s, Rosovsky [5] systematically measured the flow velocity in a curved wooden channel. Experimental studies have shown the existence of circulation in the bend, and a formula for transverse velocity distribution has been derived. Booij [6] and Blanckaert et al. [3,7] used an acoustic Doppler velocity profiler (ADVP) to accurately measure the main flow, the secondary flow and the second counterrotating secondary flow cell and correct shear stresses over a curved channel. Zeng et al. [8] confirmed the complicated nonlinear interaction between the downstream velocity and the cross-stream circulation through experiments and numerical simulation and explained the reasons for different turbulent kinetic energy at different sections. Bodnar et al. [9]discussed the elevation differences of free water surface along the channel curve through numerical simulation. These studies gave solid understanding on curved channel flows.

Aquatic vegetation is an important part of the natural riverine ecosystem and has unique ecological value, because aquatic vegetation affects hydrodynamic conditions by changing flow resistance and bed roughness [10]. Vegetation blocks the cross section of the river, resulting in different flow resistance conditions in the main river channel area and vegetation area. Water flow within vegetation has been studied since the 1950s. For example, Kouwen [11] derived a vertical distribution formula for velocity along the water depth within vegetation. Nepf and Vanoni [12] revealed that the turbulence intensity of emerged vegetation is almost uniform along the depth through flume experiments. When the vegetation is partially distributed over the channel, there is a strong shear between the nearly parallel but different flow velocities in the vegetation area and the non-vegetation area. In addition, its transverse distribution of longitudinal velocity has strong inflection points, also called mixed layer, so it is subject to Kelvin–Helmholtz (KH) instability and subsequent large-scale coherent structure (LSS) [13]. White and Nepf [14] suggested that the existence of LSS enhances the momentum exchange between the vegetated and non-vegetated areas of the channels. Therefore, the existence of LSS directly affects the velocity distribution and lateral momentum transport efficiency, which could alter the motions of sediment and nutrients on the floodplain [15,16]. Caroppi [17] experimentally found that vegetation resistance directly determines the velocity ratio of vegetation and non-vegetation areas, and LSS will disappear with the decrease of vegetation density.

For the curved channel covered with vegetation, the flow field becomes very complex due to the combination of the centrifugal force and the resistance of vegetation at the same time [18]. The vegetation reduced centrifugal effects at the bend entrance but enhanced them at the bend exit, affecting flow in the downstream bend [19]. In addition, the circulation cells caused by the secondary flow in the bend with vegetation is smaller and more spread than those observed in the non-vegetation case, which means a decrease in intensity of the cross-sectional flow [20]. Termini [21] mentioned that the turbulent quantities in vegetated meandering rivers are significantly affected by the relative vegetation submergence and different locations of the bend. Yang [22] revealed that vegetation of the convex bank increases the velocity gradient of the mixed layer larger more that of the concave bank, and both the curve and the vegetation will change the frequency of turbulence activities. Liu et al. [23] showed that the rigid emerged vegetation patches in the bend have a significant impact on the longitudinal dispersion coefficient through velocity measurement. However, the development of the mixed layer for different vegetation distribution over a curved channel is still not well understood.

Yang et al. [22] only measured the mixed layer with vegetation density 2.235% and did not discuss the effect of vegetation density on the mixed layer or large-scale vortex structure along a curved channel. Therefore, this study focuses on the changes of velocity ratio and large-scale vortex structure in the mixed layer produced by the nonuniform vegetation distribution with different vegetation densities (2.235% and 4.47%). Laboratory experiments were carried out in a 180-degree curved channel with wooden sticks simulating rigid emerged vegetation and occupying half a side of the channel. The flow characteristics such as the transverse distribution of velocity, turbulence intensity, turbulence spectrum and turbulence bursting analysis within partially distributed vegetation are analyzed using the measurements from the acoustic Doppler velocimeter (ADV). The paper is organized as follows. Section 2 describes the experimental setup and relevant parameters. In Section 3, the experimental results of velocity transverse distribution, turbulence kinetic energy, turbulence spectrum and turbulence bursting are presented, discussed and compared to reveal the influence of vegetation and curve on the mixed layer. Finally, the main conclusions are given in Section 4.

2. Materials and Methods

2.1. Experimental Apparatus

In the experiments, a 180-degree recirculating flume is used to simulate the curved river in nature. The flume is located in the Ocean Engineering Laboratory, Zhoushan Campus, Zhejiang University, China. The flume has a rectangular section made of plexiglass with width of 0.4 m and height of 0.4 m, and consists of three parts: a U-shaped curved flume, flow control system, and tailgate opening control system. The total length of the flume is 33 m, which consists of a 180-degree U-shaped curved reach with the center radius of curvature R equal to 1.4 m, a 12 m inflow straight reach and a 16 m outflow straight reach, and the constant slope of the whole flume is 0.5%. The water used in the flume is stored in the underground reservoir and recirculated by the pump. During the experiment, the feedback control system set the constant flow of 0.03 m^3/s and the constant water level at the tailgate of 0.35 m.

A three-dimensional coordinate system is established in the flume for data processing. The x, y and z flume coordinate system axes refer to the longitudinal, transverse and vertical directions, respectively. The position where $x = 0$ is at the inlet of the flume, which is positive towards the downstream; the position where $y = 0$ is the convex bank wall of the curve is positive towards the concave bank of the curve; the position where $z = 0$ is the bottom of the flume, and upward is positive. In the flume coordinate system defined above, the three-dimensional velocity components are respectively expressed as u, v and w, corresponding to the x (longitudinal), y (transverse) and z (vertical) directions.

In this experiment, a Nortek Vectrino ADV, a three-dimensional Doppler acoustic current velocimetry (ADV) with 200 Hz sampling frequency, was used to measure the three-dimensional instantaneous velocities (u, v, w). Each measuring point was continuously sampled for 120 s to ensure the accuracy and reliability of the data [24], which means about 24,000 velocity samples can be obtained at each measuring point. Through time independence verification, it is proved that the number of samples is far greater than the number required to achieve stable velocity. Therefore, the velocity samples collected in this experiment are sufficient to avoid the data measurement error caused by velocity fluctuation, so as to further eliminate the random error and improve the accuracy of velocity data.

The sampling volume of the vertical probe ADV is 0.09 cm^3, and the actual measuring point is 5 cm below the probe tip to avoid turbulence generated and the impact on the flow structure by the probe. In order to ensure the quality of the measured data, the method of Goring and Nikora (2002) was used to despike the noise [25] and remove the unqualified data with a signal-to-noise ratio (SNR) below 20 and correlation coefficient (COR) of the measured data below 70 [26].

The wooden sticks with diameter of 0.06 m and height of 0.3 m were selected to mimic emerged rigid vegetation, which is 3–5 cm higher than the water surface in the curve to achieve an emerged state. Considering that the vegetation density is close to that in nature [27], the volume density ϕ of vegetation area was set as 2.235% and 4.47%, respectively, and arranged in a regular aligned pattern [22]. The vegetation density ϕ is defined as follows:

$$\phi = \frac{1}{4}\pi ad \tag{1}$$

where a is vegetation area per unit volume, and d is vegetation diameter.

To prevent acoustic signal disturbance by the vegetation stems, two or three vegetation stems were removed when the ADV measurements were conducted. Based upon the suggestions in Caroppi et al. [28], the removal of stems over length $<3L_x$ (L_x is the spacing between two nearby stems in the streamwise direction, for $\phi = 2.235\%$ and 4.47%, $L_x = 2.5$ cm and 5 cm, respectively) has a negligible impact upon the measured velocity statistics.

Most of the vegetation in nature that grows along the meandering rivers is unevenly distributed. Therefore, three vegetation configurations were designed in the experiment to simulate this distribution pattern, which is shown in Figure 1: (i) bare-bed case (without vegetation shown in Figure 1a), (ii) convex case (vegetation was distributed half width of the channel and only along the convex bank (shown in Figure 1b), and (iii) concave case, where vegetation was distributed over a half width of the channel and only along the concave case (shown in Figure 1c).

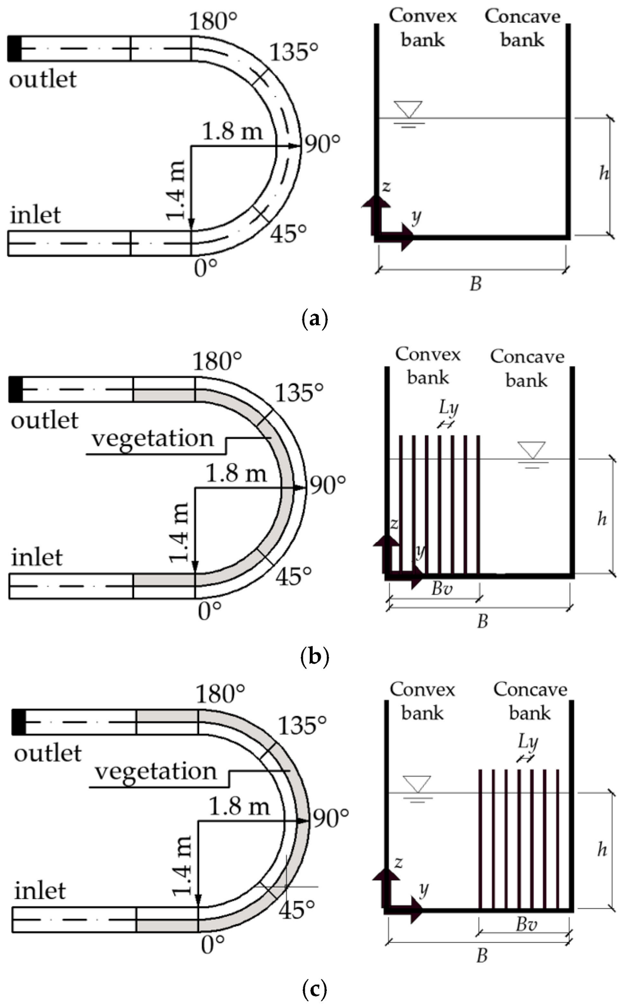

Figure 1. *Cont.*

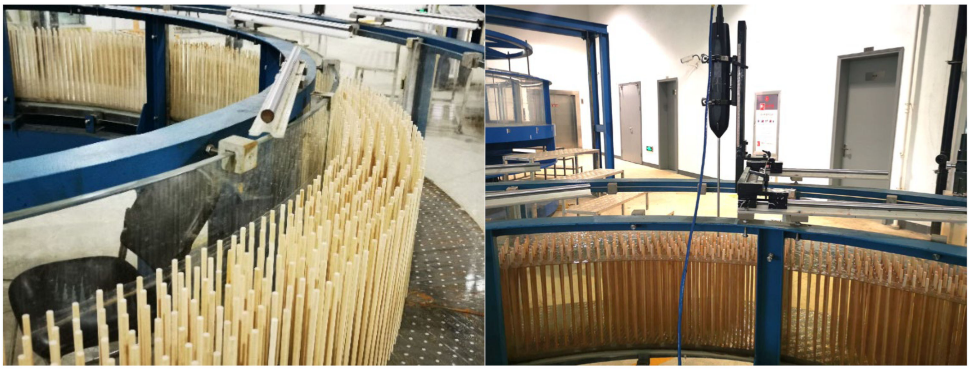

(**d**)

Figure 1. Vegetation configurations for laboratory experiments (Left: top view; Right: cross-section view, h is water depth, B is the channel width, Bv is the width of vegetation patches, and Bv/B is 1/2 in our experiments). (**a**) Bare-bed case. (**b**) Convex case (**c**) Concave case (**d**) Photos of vegetation configurations (taking the convex case as an example).

The data are measured at five selected characteristic cross sections, i.e., 0°, 45°, 90°, 135° and 180° sections. In order to discuss the influence of partly distributed vegetation on the distribution of transverse velocity, three transverse lines at each cross section were selected, which were 2 cm, 12 cm and 18 cm from the channel bed. In each transverse line, measurements were carried out every 1 cm at 10 cm to 30 cm from the convex wall and every 2.5 cm outside this region, as shown in Figure 2.

(**a**)

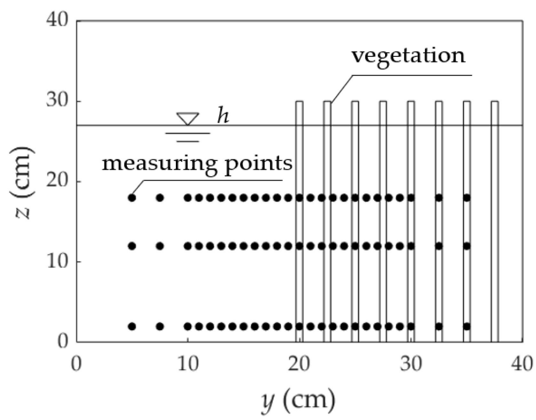

(**b**)

Figure 2. Flume picture and distribution of measuring points. (**a**) 180° U-shaped curve flume. (**b**) The schematic of the measuring points (as mentioned above, some vegetation stems are removed for ADV measurement).

2.2. Experimental Cases and Parameters

In this experiment, five experimental conditions were set up, including four cases of experimental conditions under different vegetation density and distribution location and one case of non-vegetation (bare case) conditions, which are: (i) convex case ϕ = 2.235%; (ii) convex case ϕ = 4.47%; (iii) concave case ϕ = 2.235%; (iv) concave case ϕ = 4.47%; (v) bare case.

In order to analyze the velocity distribution, U_1 and U_2 are defined as the ambient velocity within the vegetated area and the non-vegetated area respectively, i.e., $U_1 < U_2$. In the calculation, their value depends on the spatial growth characteristics, U_2 is the maximum velocity in the vegetated area (usually the velocity closest to the wall), and U_1 is the average velocity that reaches stability in the vegetation area. The convection velocity U_c, velocity difference ΔU and velocity ratio λ are defined by U_1 and U_2:

$$U_c = (U_1 + U_2)/2 \tag{2}$$

$$\Delta U = U_2 - U_1 \tag{3}$$

$$\lambda = \Delta U/2U_c \tag{4}$$

The velocity ratio λ provides the relative magnitude of the total shear compared to the convection velocity [28]. In the canonical plane mixing layer, the velocity ratio λ controls the spatially growing characteristics of the mixing layer [29]. The mixed layer develops to be stable at a certain distance from the shear origin. This development trend is not only limited by the resistance from the channel bed, the lateral limit of the side wall, and the vertical limit of the flow surface [30], but also related to the density of vegetation, the circulation in the bend and other factors. The λ value is used for quantitative analysis in this study.

The momentum thickness of the vegetation mixed layer is defined as:

$$\theta = \int_0^B \left\{ \frac{1}{4} - \left[\frac{U(y) - U_c}{\Delta U} \right]^2 \right\} dy \tag{5}$$

where $U\,(y)$ is the transverse distribution of longitudinal velocity u, and the width of a shear layer δ is defined as the distance between positions where velocity difference $\Delta\ U$ reaches 10% and 90% of the ambient flow value [31]. The Reynolds number based on mixing layer thickness Re_θ and water depth Re_h can be defined as:

$$Re_\theta = \Delta U \theta / \nu \tag{6}$$

$$Re_h = U_2 h / \nu \tag{7}$$

where ν is the kinematic viscosity of water.

Table 1 provides the important parameters obtained from experiments.

Table 1. Results of the experiment.

Case	1 (Convex Case)					2 (Convex Case)				
Section	0°	45°	90°	135°	180°	0°	45°	90°	135°	180°
Density	2.24%	2.24%	2.24%	2.24%	2.24%	4.47%	4.47%	4.47%	4.47%	4.47%
$h(m)$	0.258	0.262	0.269	0.273	0.278	0.254	0.255	0.258	0.262	0.266
$U_1(m/s)$	0.1655	0.1332	0.1169	0.0970	0.0830	0.0809	0.0541	0.0505	0.0500	0.0494
$U_2(m/s)$	0.4339	0.4779	0.4754	0.4718	0.4700	0.4534	0.4737	0.4379	0.4288	0.4439
$U_C(m/s)$	0.2997	0.3056	0.2962	0.2844	0.2765	0.2672	0.2639	0.2442	0.2394	0.2467
$\Delta U\ (m/s)$	0.2684	0.3447	0.3585	0.3748	0.3870	0.3725	0.4196	0.3874	0.3788	0.3945
$\delta(m)$	0.08	0.10	0.11	0.12	0.14	0.07	0.11	0.13	0.14	0.15
$\theta(m)$	0.0400	0.0348	0.0304	0.0317	0.0376	0.0218	0.0266	0.0297	0.0342	0.0356
λ	0.45	0.56	0.61	0.66	0.70	0.70	0.79	0.79	0.79	0.80
Re_θ	10736	11996	10898	11881	14551	8121	11161	11506	12955	14044
Re_h	111946	125210	127883	128801	130660	115164	120320	112978	112346	118077
Re_θ/Re_h	0.10	0.10	0.09	0.09	0.11	0.07	0.09	0.10	0.12	0.12

Table 1. *Cont.*

Case	3 (Concave Case)					4 (Concave Case)				
Section	0°	45°	90°	135°	180°	0°	45°	90°	135°	180°
Density	2.24%	2.24%	2.24%	2.24%	2.24%	4.47%	4.47%	4.47%	4.47%	4.47%
$h(m)$	0.260	0.264	0.267	0.274	0.278	0.255	0.262	0.263	0.267	0.272
$U_1(m/s)$	0.1500	0.1024	0.1192	0.1183	0.1423	0.0590	0.0379	0.0456	0.0449	0.0433
$U_2(m/s)$	0.4659	0.4891	0.4223	0.4602	0.4467	0.3477	0.3867	0.3049	0.2978	0.2773
$U_C(m/s)$	0.3080	0.2958	0.2708	0.2893	0.2945	0.2034	0.2123	0.1752	0.1714	0.1603
ΔU	0.3159	0.3867	0.3031	0.3419	0.3044	0.2887	0.3488	0.2593	0.2529	0.2339
$\delta(m)$	0.14	0.15	0.17	0.16	0.16	0.08	0.11	0.07	0.09	0.07
$\theta(m)$	0.0414	0.0376	0.0330	0.0327	0.0346	0.0233	0.0291	0.0221	0.0242	0.0224
λ	0.51	0.65	0.56	0.59	0.52	0.71	0.82	0.74	0.74	0.73
Re_θ	13078	14540	10002	11180	10532	6727	10150	5731	6120	5239
Re_h	127657	134992	116133	126095	120609	88664	101315	80189	79513	75426
Re_θ/Re_h	0.10	0.11	0.09	0.09	0.09	0.08	0.10	0.07	0.08	0.07

3. Results

3.1. Transverse Velocity Distribution

Figure 3 shows the transverse distribution of longitudinal velocity for different cases. The abscissa is the normalized width y/B, where B (=0.4 m) is the width of the flume. The ordinate is the longitudinal velocity, and its value is the average velocity of 120 s measured by ADV. The blue vertical dotted line in the figure indicates the boundary between the vegetation area and the non-vegetation area, that is, the center line of the flume, 20 cm from the convex bank.

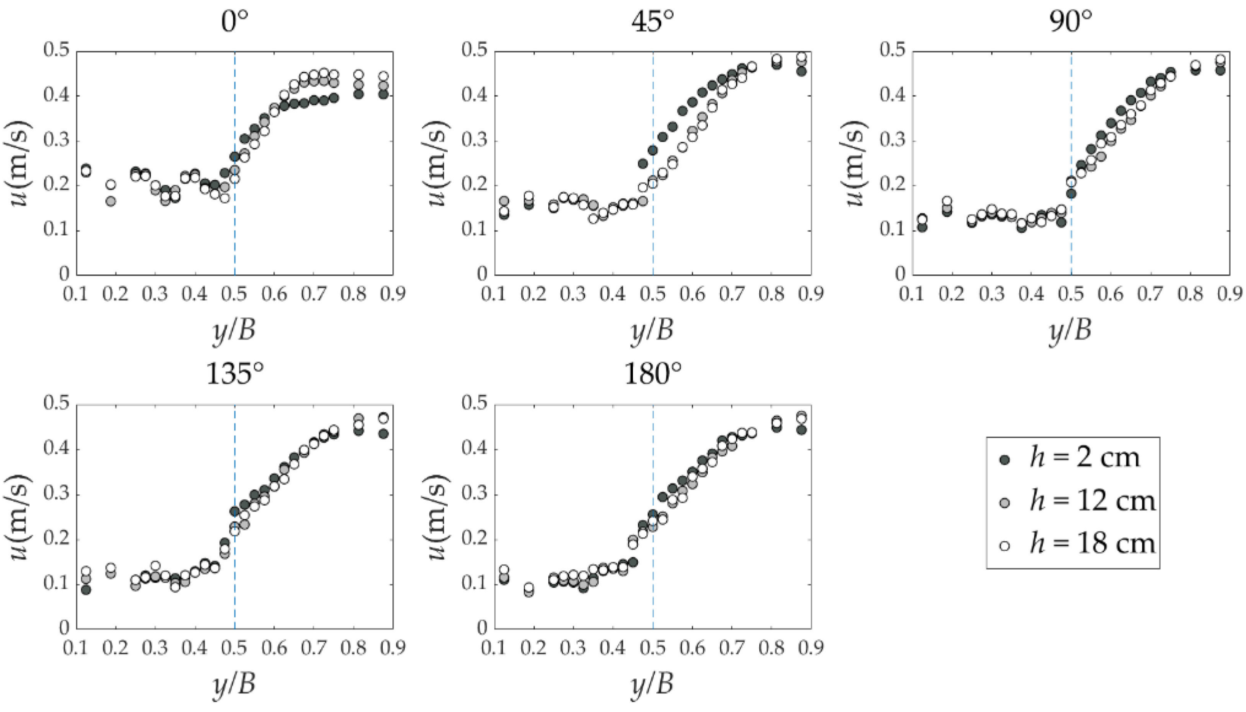

(**a**)

Figure 3. *Cont.*

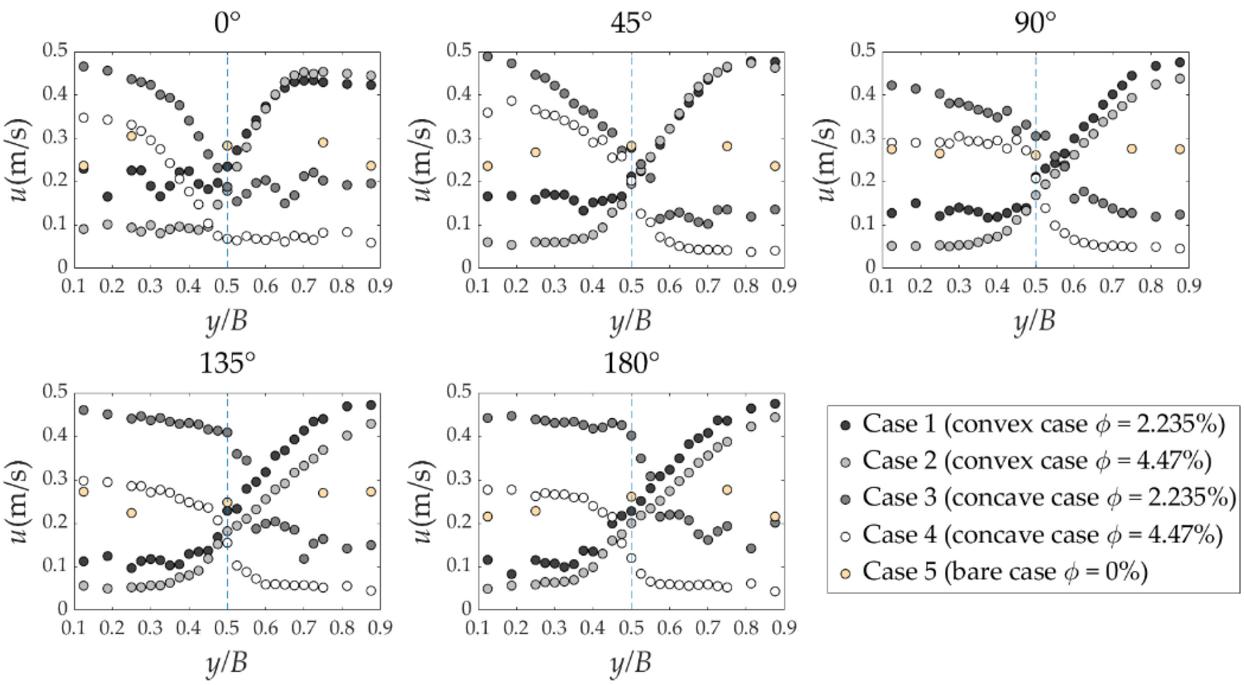

(**b**)

Figure 3. Longitudinal velocity distribution along transverse direction on five cross sections. (**a**) Transverse distribution of longitudinal velocity at different vertical positions in Case 1 (**b**) Transverse distribution of longitudinal velocity at z = 12 cm for different cases.

Case 1 was taken as an example to show the influence of vertical positions in five characteristic sections on the transverse distribution of longitudinal velocity in Figure 3a. For each section along the curve, the longitudinal velocity is generally small in the vegetation area but large in the non-vegetation area. In addition, there is an obvious velocity gradient between vegetation and non-vegetation areas as in the case of a straight channel [17]. The results also show that the transverse distribution of velocity at different depth is basically similar, and there is a small velocity difference only near the side wall, for the wall effect is greater than the vegetation resistance. It implies that the change in vertical depth position does not have an impact on the trend of transverse velocity distribution and the velocity in the mixed layer when a rigid round stick with vertically uniform resistance was used as simulated vegetation. Therefore, the medium depth survey line of z = 12 cm from the bottom was taken as an example to analyze the test cases.

The results in Figure 3b show that the velocity distribution was jointly affected by the effects of vegetation density and vegetation distribution and the curve effect. For the same distribution cases, velocity along the transverse direction for Cases 1 and 3 (ϕ = 2.235%) is significantly larger than that for Cases 2 and 4 (ϕ = 4.47%), indicating that the vegetation resistance is still the main factor to affect the velocity. However, for the same difference in vegetation resistance, the variation in velocity in the concave case (the difference of velocity between Cases 2 and 4) is considerably greater than that in convex case (the difference of velocity between cases 1 and 3). It can be seen that the response of velocity to the change of vegetation density in the concave bank is faster. In addition, when vegetation density is the same in the concave or convex bank, the velocity distribution for the concave and convex bank is symmetrical with respect to the vegetation boundary (i.e., y/B = 0.5) for sparse vegetation (ϕ = 2.235%). On the other hand, when the vegetation density is greater (ϕ = 4.47%), the velocity distribution for the concave and convex cases is no longer symmetrical. The velocity U_1 in the vegetation area is still similar, but there is a significant difference in the velocity U_2 in the non-vegetation area. For example, U_2 at the 0 ° section of case 2 is 0.4534 m/s, while for Case 4 it is 0.3477 m/s. This result reveals that the change of vegetation density on convex bank and concave bank has different effects on transverse velocity distribution as [22] mentioned.

The effect of the channel bend on velocity distribution is mainly represented by the secondary flow. The velocity U_1 has almost no significant change in the vegetation area of each section during the development along the curve, but the velocity U_2 in the non-vegetation area of the convex case gradually increase from the 0° section to180° section. The decrease along the curve of the velocity difference ΔU (in Table 1) also proves the maximum velocity U_2 was not completely developed. This trend mainly appears in the velocity of concave area, while the velocity of convex area is not affected by the curve. This is possibly due to the secondary flow induced by the channel bend.

For all experimental cases, the velocity ratio λ that characterizes the mixing layer ranges between 0.45~0.81, which is greater than 0.3 [16,32], the threshold to initiate the K-H instability. It is confirmed that K-H instability exists in all experimental cases, and there is an inflection point of transverse velocity profiles and large velocity gradient. Therefore, this research is applicable to the mixed layer theory affected by the K-H instability [33].

Since there is an inflection point in the shear section of the velocity distribution, the shape is similar to the standard hyperbolic tangent function of the mixed layer:

$$\frac{U-\overline{U}}{\Delta U} = 0.5\tan\mathrm{h}\left(\frac{y-\overline{y}}{2\theta}\right) \tag{8}$$

Cases 2 and 4 with large vegetation density were taken as examples to compare the measured data with the theoretical formula in Equation (8), as shown in Figure 4. The points in Figure 4 are the measured data of different vertical positions, and the blue line is the theoretical curve. The results in Figure 4 show that the transverse distribution of the measured longitudinal velocity is in good agreement with the hyperbolic tangent function of the mixed layer, suggesting the similarity of the mixed layer in straight reach and curved reach (both convex and concave cases).

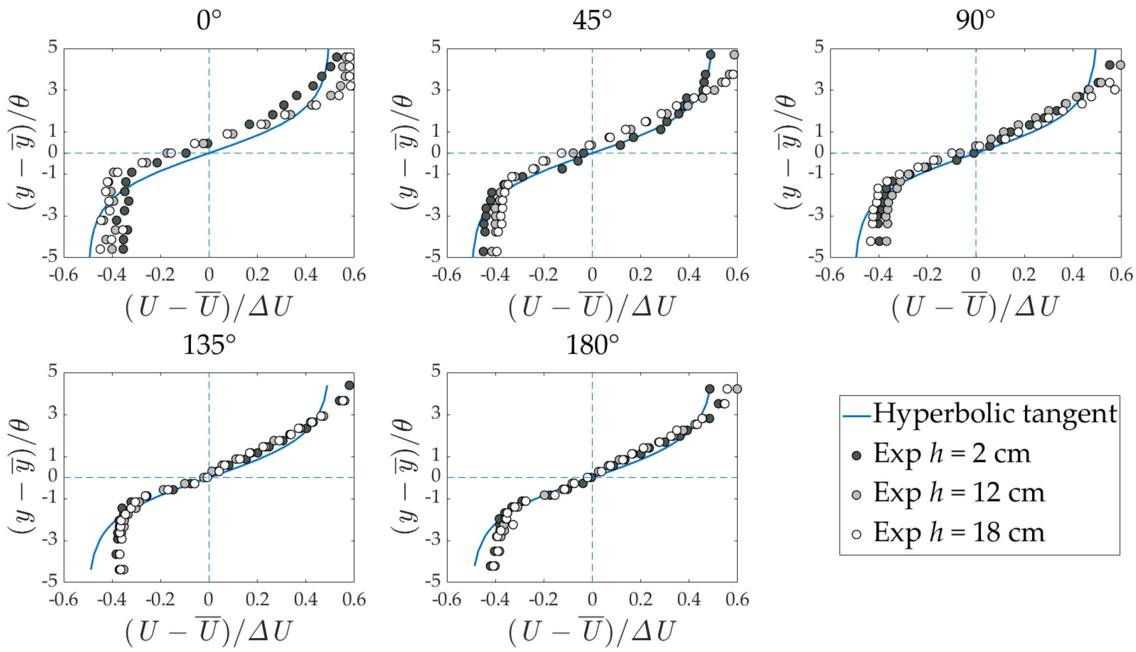

(**a**)

Figure 4. *Cont.*

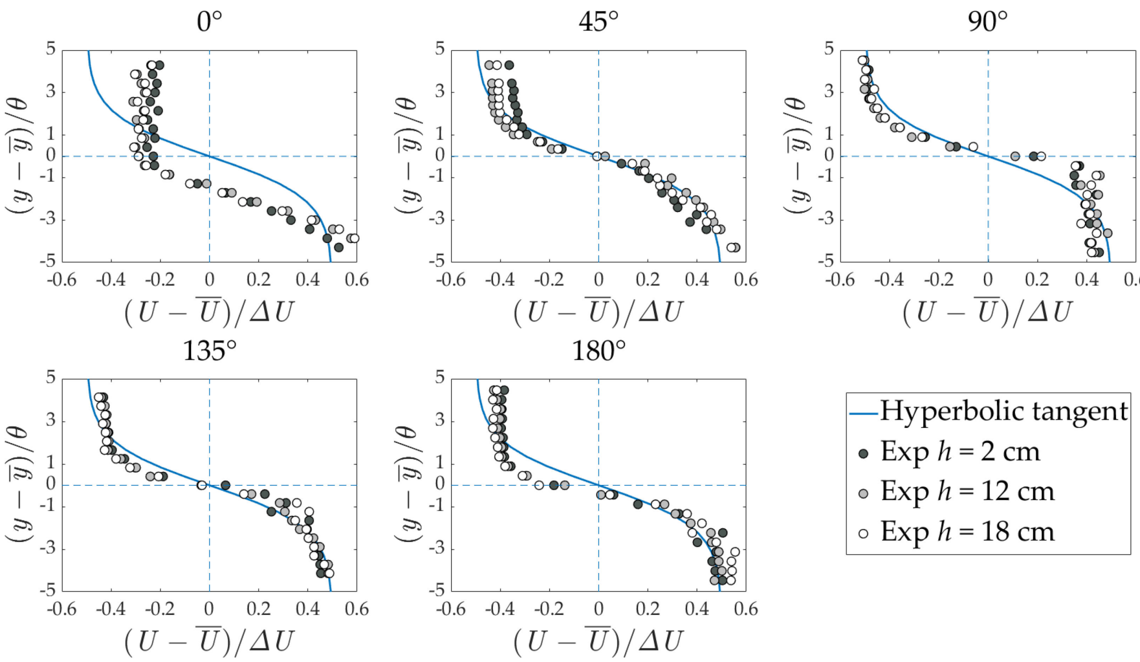

(**b**)

Figure 4. Fitting of transverse velocity distribution for different vegetation distribution. (**a**) Convex case. (**b**) Concave case.

Compared with the fitting results of the concave case in Figure 4b, the results of the convex case shown in Figure 4a are located slightly above the theoretical hyperbolic tangent curve, while the values in the concave case are below the theoretical curve. The result of the convex case with the range $-0.4 < (U-\overline{U})/\Delta U < 0.4$ is better fit to the theoretical curve, especially at the 135° and 180° sections, while the fitting degree of the concave case at both ends of the abscissa ($(U-\overline{U})/\Delta U < -0.4$ and $(U-\overline{U})/\Delta U > 0.4$) is better in the latter part of the curve. This is mainly because the centrifugal force points to the concave bank in the curve, and the velocity ratio λ of the convex case is larger than that in the concave case.

In addition, the thickness θ of the mixed layer with vegetation density ϕ = 2.235% is basically larger than that with ϕ = 4.47%, which decreases first and then increases along the curved channel, and finally reaches the minimum in the middle section of the curved channel, as shown in Figure 5. For the Cases 2 and 4 (ϕ = 4.47%), the thickness θ of the convex case increases along the section, while that of the concave case has little change in each section. The phenomenon is mainly due to the difference in longitudinal velocity distribution between the convex and concave cases, as previously described.

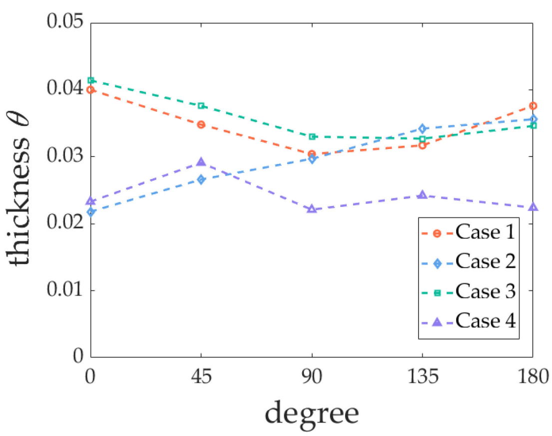

Figure 5. The variation of the momentum thickness θ along the channel curve.

3.2. Turbulence Intensity Analysis

In the section, *TKE* (turbulence kinetic energy) is used to estimate the intensity of turbulence, which is defined by:

$$TKE = \frac{1}{2}\left(\overline{u'^2} + \overline{v'^2} + \overline{w'^2}\right) \tag{9}$$

where u', v' and w' are, respectively, x, y and z three-dimensional fluctuating velocity, which is $u' = u - \overline{u}$, $v' = v - \overline{v}$ and $w' = w - \overline{w}$, and $\overline{u}$,$\overline{v}$,$\overline{w}$ is the three-dimensional time average velocity.

Figure 6 analyzes *TKE* for different cases and cross sections, taking ADV measurements at h = 12 cm as an example. For Case 5 (bare bed, Figure 6e), *TKE* increases as the flow goes into the curved part, and *TKE* at y/B = 0.5 reaches the peak at the 135 ° section while *TKE* at y/B = 0.75 reaches the peak at the 180° section, indicating that the strongest turbulence mainly occurs at the section. In addition, the *TKE* of the curved section is greater than that of the straight section, which means that the curved section enhances the turbulent intensity by promoting the mixing of water flow. This result is consistent with the results of Termini [34] and Yang et al. [22].

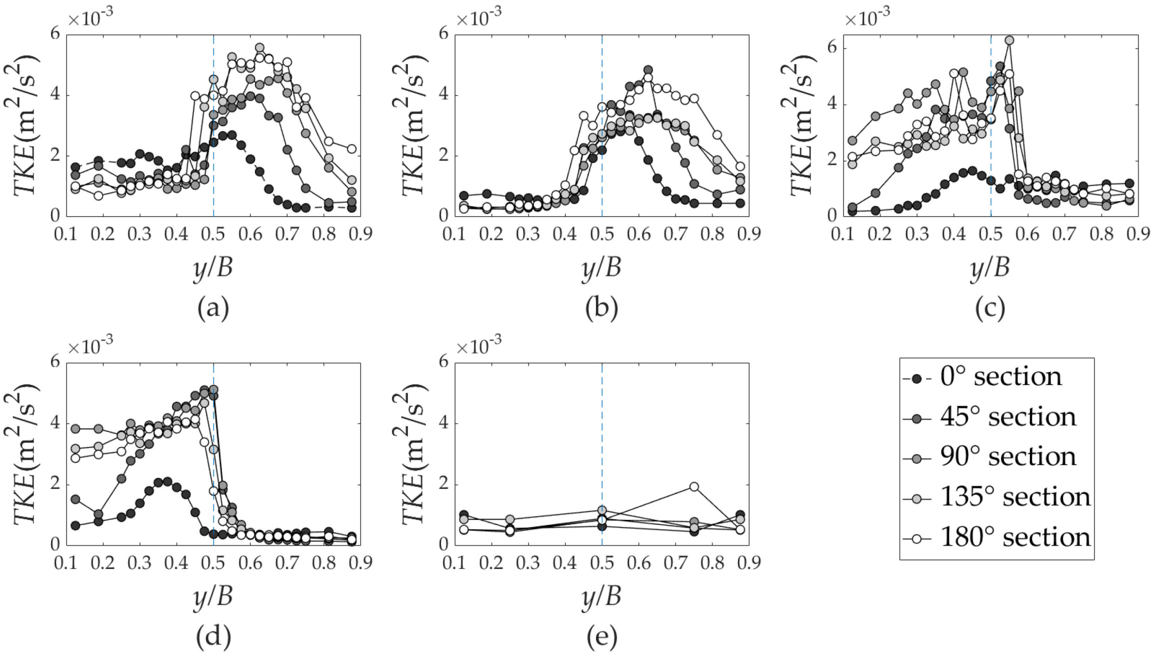

Figure 6. Turbulent kinetic energy distribution at five cross sections: (**a**) Case 1; (**b**) Case 2; (**c**) Case 3; (**d**) Case 4; (**e**) Case 5.

For Cases 1 to 4, the minimum *TKE* of each section appears in the vegetation area (y/B < 0.4 in Cases 1 and 2 of vegetation distributed along the convex bank and y/B > 0.6 in Cases 3 and 4 of vegetation placed along the concave bank), and reaches a stable value close to the turbulent kinetic energy of Case 5, which is approximately 0.001 m^2/s^2 in each section. The TKE in the vegetation zone of both Case 2 and Case 4 were lower than that of Case 5. The result shows that the vegetation with $\phi = 4.47\%$ can inhibit turbulence in the vegetation zone, leading to the reduction in TKE, which is different from the vegetation with $\phi = 2.235\%$. Compared with the vegetation arranged on convex bank, the vegetation arranged on the concave bank has a stronger inhibition effect. However, the peak values of *TKE* appear near the non-vegetation area at the lateral interface between vegetation and non-vegetation areas (0.5 < y/B < 0.7 in the convex case, 0.4 < y/B < 0.5 in the concave case). This phenomenon is due to the existence of large velocity gradient and inflection point of longitudinal velocity profile in this area.

By comparing the peak *TKE* values for different cases, it is found that the influence of the location along a curved channel is greater than that from vegetation density and distribution on peak *TKE* values. For the convex case, the ratio of the peak *TKE* values between 180° and 0° sections is 1.5~2, while the ratio becomes 3~5 for the concave case, indicating that the vegetation occupied along the concave bank has a greater impact on the turbulent characteristics. This is because the combined effect of vegetation and channel curve enhances the mixing between water bodies, and the wake effect of vegetation flow is amplified by the bend, further elevating the turbulence of water bodies. Furthermore, the centrifugal force pointing at the concave bank intensifies the turbulence intensity on the concave bank. Since the peak values of *TKE* of the convex case appear in the non-vegetation area near the concave bank, the peak value is not only larger and deeper into the non-vegetation area than that of the concave case, but also decays in a slower rate. Therefore, the region of peak *TKE* values perform a round shape for Cases 1 and 2 and exhibits a spike shape for Cases 3 and 4, as shown in Figure 6.

The change in vegetation density will alter vegetation resistance, subsequently affecting the *TKE*. When the vegetation is denser, the *TKE* values become smaller, and the transverse position of the *TKE* peak will shift to the non-vegetation area. The maximum *TKE* value appears at the 135° section for cases with ϕ =4.47%, while the maximum turbulent kinetic energy can be found at 45 ° section for cases with ϕ = 2.235% density, which does not affect the variation in *TKE*. However, the change of the transverse position where the peak *TKE* value appears indicates that the *TKE* is comprehensively affected by the vegetation density, distribution and channel curve.

3.3. Power Spectral Density Analysis

The turbulence spectrum gives the occurrence possibility F (f) (i.e., the spectral density) of turbulent eddies with different frequency f at a fixed point. The spectral analysis is based on the Welch method [35] with Hamming-type windowing [36] (using commercial software Matlab, Mathworks). The high-frequency part represents small-scale turbulence vortex and the low-frequency part denotes large-scale turbulence vortex in the turbulence spectrum. The structure of turbulence vortex, and the transport and dissipation of *TKE* can be understood through spectral analysis [37]. Figures 7 and 8 show the variation in power spectral density (PSD) S_{vv} of the lateral fluctuation velocities measured by 200 Hz ADV with different frequency f. The noise in the turbulence spectrum is removed by the moving average method.

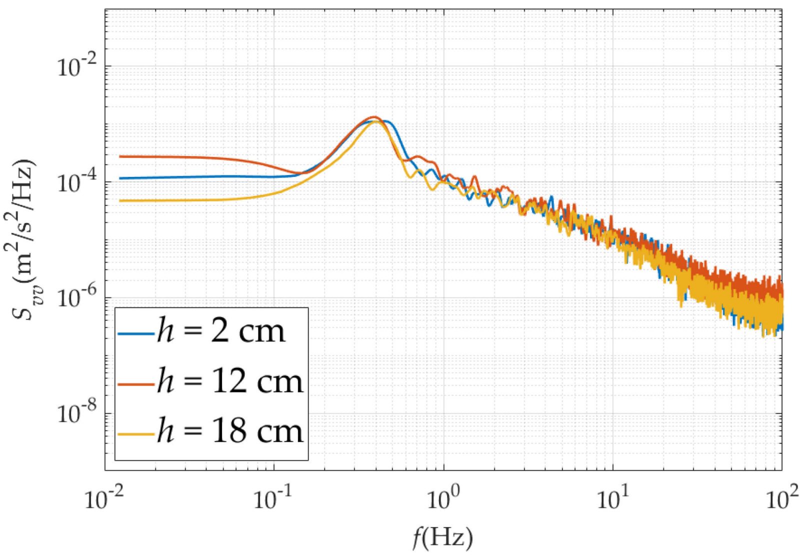

Figure 7. PSD of different depths at the centerline of the 45° section for Case 2.

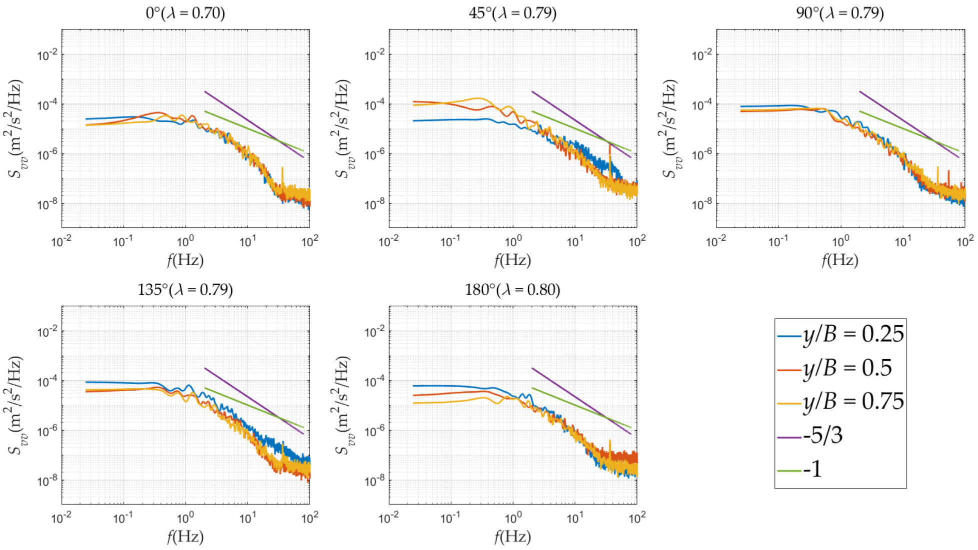

(**a**) Bare-bed case (Case 5)

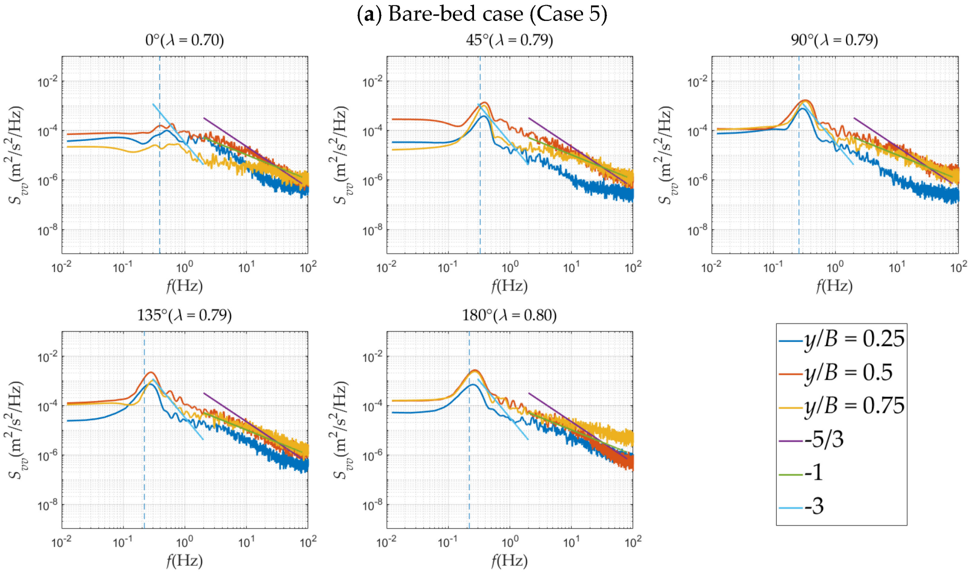

(**b**) Convex case (Case 2)

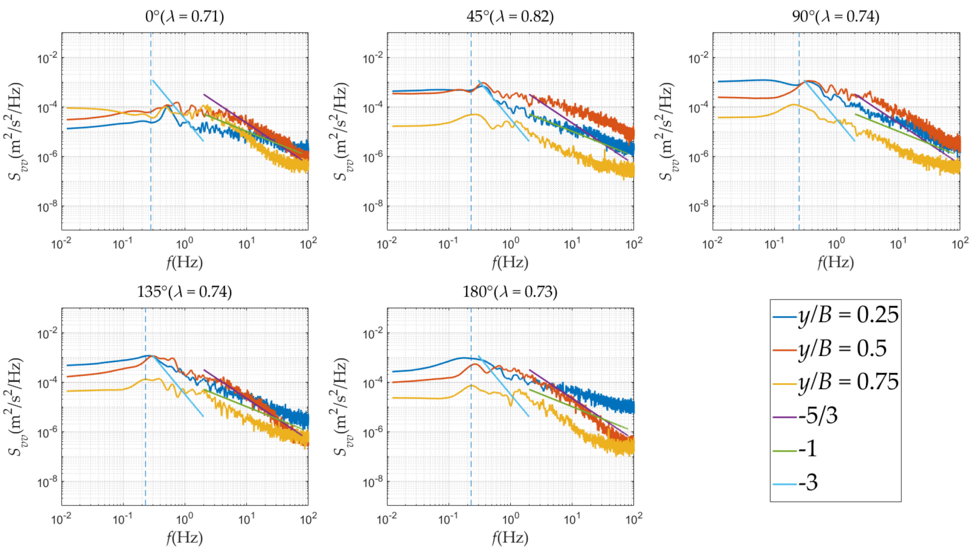

(**c**) Concave case (Case 4)

Figure 8. PSD at different sections of convex and concave cases.

To understand the effect of depth on PSD, the data of three depths (h = 2 cm, 12 cm, and 18 cm from the bottom) at the center line of the 45° section for Case 2 (λ = 0.79) are compared in Figure 7. It can be seen from the figure that the PSD in the inertial subrange and dissipation range at different heights is similar but shows certain differences in the energetic range (PSD in h = 12 cm > PSD in h = 2 cm > PSD in h = 18 cm). This result indicates that the turbulence vortex structure along the vertical direction is approximately the same with a certain difference only in the large-scale vortex. Therefore, only the PSD at middle position (h = 12 cm) is analyzed afterwards.

Figure 8 displays the variation of PSD of lateral fluctuation velocity for Cases 2 and Case 4, and the velocity ratio of each section λ was provided as well. For each case, the PSD at the vegetation and non-vegetation interface area (y/B = 0.5) is the largest, which is due to the strongest interaction between vegetation and water in this area and the greater turbulence intensity, consistent with the *TKE* results in the previous section. The spectrum in vegetation areas and non-vegetation areas has no obvious trend in the energetic range, but the PSD in vegetation areas (y/B = 0.25 in Figure 8a and y/B = 0.75 in Figure 8b) reaches the minimum value in the dissipation range among the three regions, suggesting that the small-scale turbulence in vegetation area is the least, while there are more small-scale turbulence eddies in the interface area and non-vegetation area. Additionally, the PSD peak in the convex case is more obvious than that in concave case.

The attenuation rate of the PSD is compared with several characteristic slopes in the classical turbulence spectral density plot, where the blue line represents f^{-3}, the green line denotes f^{-1}, and the purple line means $f^{-5/3}$. In the bare-bed case in Figure 8, the attenuation rate of the PSD in the dissipation region of each section from 0° to 180° is consistent with Kolmogorov's law ($k = -5/3$), indicating that the curve does not affect the attenuation of energy. However, the PSD at the 0° section is different from curve sections in the convex case and concave case. At the 0° section, the attenuation rate in the vegetation area (y/B = 0.25 in the convex case and y/B = 0.75 in the concave case) is still $k = -5/3$, but in the non-vegetation area the rate is changed to $k = -1$, and at the interfacial area, the rate ranges between $k = -1$ and $k = -5/3$. In curve sections, the attenuation rate is basically close to $k = -1$ and considerably different from $k = -5/3$ proposed by Kolmogorov's law, which is consistent with the results obtained by Huai et al. [36]. The result may be due to the existence of vegetation in the curved channel, which leads to the decrease in turbulent eddies, the increase of small-scale turbulent vortex and the energy dissipates at a greater rate than that in a straight channel because of viscous friction. In addition, the attenuation rate of the curve sections varies in different regions, and it can be ranked as: k (non-vegetation area) > k (vegetation area) > k (interfacial area), and at the interface area k is more consistent with Kolmogorov's law.

The turbulent motion is strongest at the interfacial area, and the mixing layer in the interfacial area is affected by Kelvin–Helmholtz (KH) instability, generating a K-H vortex. The peak frequency f_{KH} of the dominant K-H vortex at this area obtained from Figures 7 and 8 varies between 0.2 and 0.4 Hz. The relationship between the peak frequency f and the momentum thickness of the mixing layer θ is described by the Strouhal number (St) as given below.

$$St = \frac{f\theta}{U_c} \tag{10}$$

The classical St value in the standard mixing layer is 0.032 [37]. The momentum thickness of the mixed layer and the frequency of K-H instability of convex and concave cases are listed in Table 2. In the table, f represents the frequency calculated from St = 0.032 in the turbulence spectrum, which is obtained by Equation (10) and represented by the vertical blue dotted line in Figure 8. f_{KH} is the peak frequency determined from experiments, i.e., the dominant vortex frequency of the mixing layer in the curved channel. The comparison in Figure 8 shows that the measured peak frequency f_{KH} is in good agreement with the theoretical frequency f, which proves that the large-scale vortex structure existing at the interfacial area of the curved channel is the K-H vortex. In some sections, $f < f_{\mathrm{KH}}$ is due to the value of U_c is rather small. The K-H vortex peak frequency f_{KH} in the experiment is the largest at the 0° section and the smallest at the 180° section irrespective of vegetation arrangement, and it decreases gradually as flow moves into the curved part of the channel, indicating that the curved channel promotes the development of turbulence and increases the K-H vortex in the mixed layer.

Table 2. The momentum thickness and K-H instability frequency for Cases 2 and 4.

	Case	0°	45°	90°	135°	180°
$\theta(m)$	2(Convex case)	0.0218	0.0266	0.0297	0.0342	0.0356
	4(Concave case)	0.0233	0.0291	0.0221	0.0242	0.0224
f	2(Convex case)	0.39	0.32	0.26	0.22	0.22
	4(Concave case)	0.28	0.23	0.25	0.23	0.23
$f_{KH}(Hz)$	2(Convex case)	0.42	0.40	0.35	0.29	0.27
	4(Concave case)	0.44	0.39	0.30	0.25	0.22

The 90° and 135° sections in the second half of the curve were taken as an example to show the influence of vegetation density on turbulence spectrum in the curve, as shown in Figure 9. The measured points in the Figure 9 were located at the middle depth, 12 cm away from the bottom bed. It can be seen from the figure that the peak frequency at the interfacial area is 0.6~0.7 Hz for Case 1 (ϕ = 2.235%), while the peak frequency at the interfacial area becomes 0.1~0.4 Hz for Case 3 (ϕ = 4.47%), which is obviously lower than the peak frequency for Case 1 (sparse vegetation). It is the same conclusion as the rigid vegetation experiment of Caroppi [17], that is, the peak frequency gradually increases with the decrease in vegetation density. This is because the decrease of vegetation density leads to the decrease of velocity ratio λ, which changes the turbulent structure and frequency of vortex in the mixed layer.

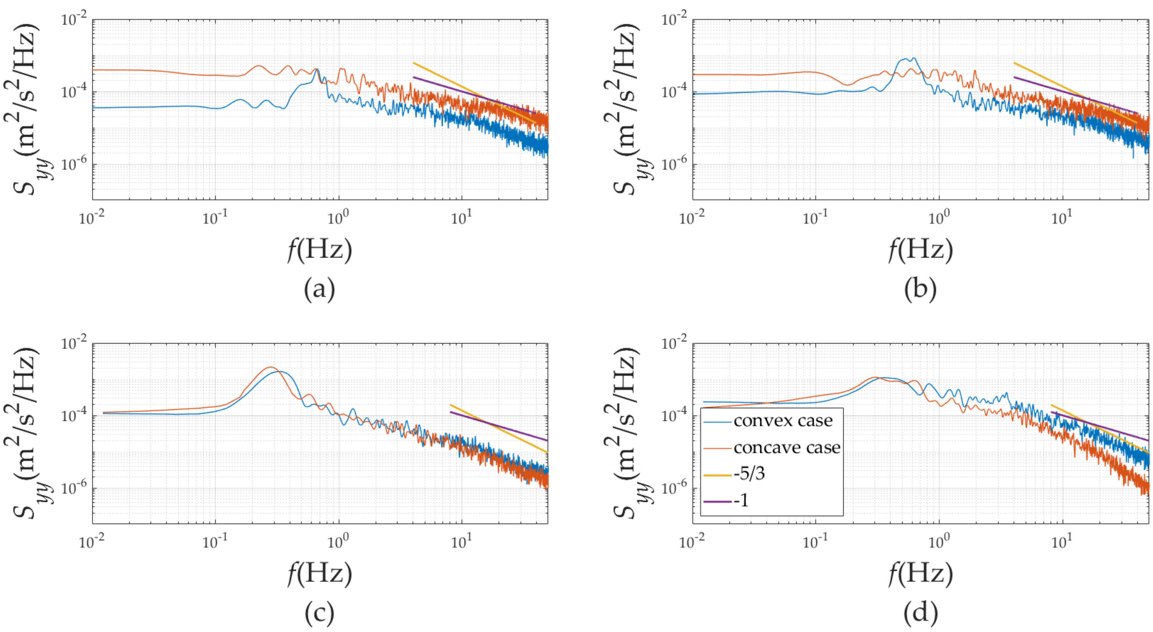

Figure 9. Effect of vegetation density on turbulent spectrum: (**a**) ϕ =2.235% at the 90°section; (**b**) ϕ = 2.235% at the 135°section; (**c**) ϕ = 4.47% at the 90°section; (**d**) ϕ = 4.47% at the 135 section.

Furthermore, there is no significant difference for the PSD values of convex and concave cases when the vegetation density ϕ is 4.47%, which reveals that the effect of dense vegetation plays a more important role on turbulent structure than the curved channel does.

However, the peak value of the concave case is not evident when the vegetation density ϕ is 2.235%.

3.4. Turbulent Bursting

The quadrant analysis was used to clarify the influence of vegetation density, distribution form, and channel curve on coherence structure near the bed. In turbulence bursting, four types of contribution to Reynolds stress are classified according to the sign of instantaneous fluctuating velocity u' and w', as follows [38]:

The first quadrant (Q1): $u' > 0$, $w' > 0$ is the outward interaction;

The second quadrant (Q2): $u' < 0$, $w' > 0$ is the ejection;

The third quadrant (Q3): $u' < 0$, $w' < 0$ is the inward interaction;

The fourth quadrant (Q4): $u' > 0$, $w' < 0$ is the sweep.

Each quadrant can represent a type of turbulence event. A threshold value H_0 was set to remove the influence of small values in quadrant analysis. Only the Reynolds stress contribution greater than this threshold in each quadrant was calculated [39]. This threshold value is reflected in the quadrant as four hyperbolas that replace 0, that is, $|u\prime(\mathrm{t})w\prime(\mathrm{t})| \geq H_0\ |\overline{u\prime w\prime}|$, where $u'\ w'$ represents the Reynolds stress. The contribution of each quadrant is represented by S_k, where k = I, II, III, IV represents four quadrants:

$$S_k = \begin{cases} 1, |u'(t)w\prime(t)| \geq H_0|\overline{u\prime w\prime}| \\ 0, |u'(t)w\prime(t)| < H_0\ |\overline{u\prime w\prime}| \end{cases} \tag{11}$$

In this section, the threshold value H_0 = 1.0 [40,41] and the occurrence frequency f_k of turbulence events in the four quadrants can be expressed as:

$$f_k = \frac{\sum_{t=0}^{T} S_k}{\sum_{t=0}^{T} S_I + \sum_{t=0}^{T} S_{II} + \sum_{t=0}^{T} S_{III} + \sum_{t=0}^{T} S_{IV}} \tag{12}$$

where T is the recording period.

Figure 10 shows the occurrence frequency of different turbulence events at different cross section when vegetation is present on the convex bank or concave bank. Vegetation density ϕ =4.47% was taken as the example so that the result was more obvious than the case of ϕ =2.235%. The measuring points were all located at 2 cm from the bottom bed.

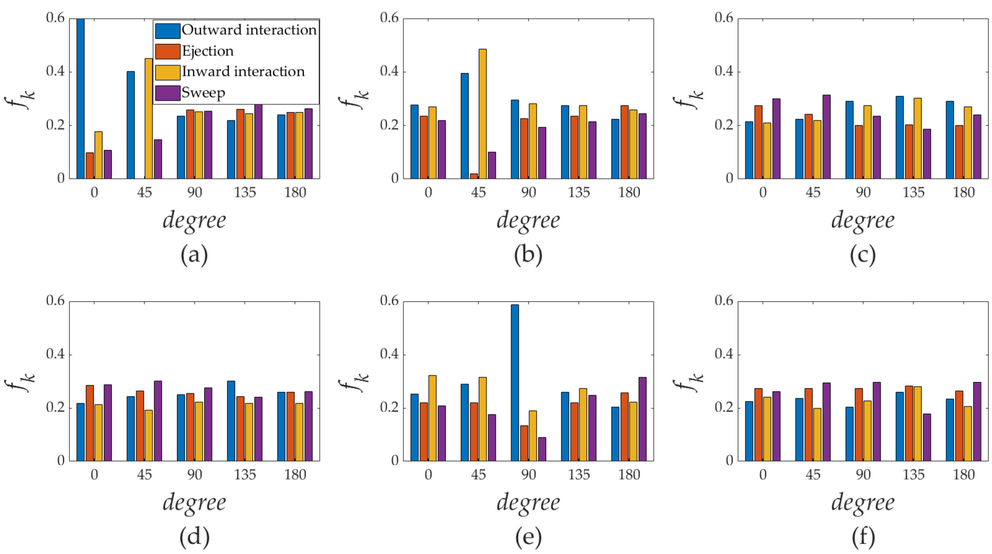

Figure 10. Frequency of occurrence of coherence turbulent events for: (**a**) Case 2 in vegetation areas (y/B = 0.25); (**b**) Case 2 at interfacial areas (y/B = 0.5); (**c**) Case 2 in non-vegetation areas (y/B = 0.75); (**d**) Case 4 in non-vegetation areas (y/B = 0.25); (**e**) Case 4 at interfacial areas (y/B = 0.5); (**f**) Case 4 in vegetation areas (y/B = 0.75).

Figure 10b,e show that the occurrence frequency of the inward interaction and outward interaction at the interface from the 0° to 135° section is greater than the frequency of ejection and sweep, which is the same as that of the vegetation occupied in the straight channel [42]. The reason is that the near-bed Reynolds stresses with vegetation are generally lower than that without vegetation, because the inward and outward interactions that dominant turbulence activities have negative contribution on Reynolds stress. The inward interaction and outward interaction dominate the turbulent bursting, which indicates that the vegetation in the curved channel also changes Reynolds stress contribution. At the 180° section, the frequency ratio of ejection and sweep increases, possibly due to the influence of the curve.

For Figure 10c,d (in the non-vegetation areas), the ejection and sweep events play a dominant role in turbulent bursting, similar to the turbulent events in the non-vegetation flow of a straight channel. In the vegetation area of the convex case, the turbulence event in the first half of the bend is obviously dominated by inward and outward interactions, while the contribution of ejection and sweep to Reynolds stress increases with the development of the bend, and the final contribution from four turbulence events is similar. However, the results of the vegetation area for the concave case are different from other areas affected by vegetation, and the Reynolds stress contribution is not determined by inward and outward interactions, but by ejection and sweep.

The turbulent bursting in the non-vegetation area of convex and concave cases is consistent with the bare-bed case in Yang's study [22]: the occurrence frequency of sweep and ejection is higher at the 0° section, but the frequency of inward and outward interactions gradually increases under the influence of the curve, and the frequency of occurrence for the four events is similar at the 180° section. However, the frequency of the four turbulence events after the 90° section is approximately the same in the vegetation and interfacial area affected by vegetation ($\phi = 4.47\%$), which also happens after the 45° section in Yang's vegetation interfacial area ($\phi = 2.235\%$). This is because the Reynolds stress at the bottom of the vegetation area is smaller, and the contribution of each type of Reynolds stress is relatively uniform. This special phenomenon reflects that the joint impact of curved and half-sided vegetation on turbulent bursting events is complicated.

The bursting phenomenon also can be assessed according to the skewness coefficients [43], which can provide the information of the material exchange between vegetation area and non-vegetation area. Skewness coefficients are defined as:

$$Sk_x = \frac{1}{N}\sum_{i=1}^{N} u^3 / \left(\sqrt{\frac{1}{N}\sum_{i=1}^{N} u^2}\right)^3 \quad (13)$$

$$Sk_y = \frac{1}{N}\sum_{i=1}^{N} v^3 / \left(\sqrt{\frac{1}{N}\sum_{i=1}^{N} v^2}\right)^3 \quad (14)$$

where N is the sampling number, Sk_x and Sk_y are the skewness coefficients of u and v, respectively. The four types of contribution to Reynolds stress mentioned above can be described by skewness coefficients: outward interaction ($Sk_x > 0$, $Sk_y > 0$), ejection ($Sk_x < 0$, $Sk_y > 0$), inward interaction ($Sk_x < 0$, $Sk_y < 0$) and sweep ($Sk_x > 0$, $Sk_y < 0$).

Figure 11 shows the lateral distribution of skewness coefficients at h = 12 cm. For the Cases 2 and 4 (ϕ =4.47%), the sweep and ejection can be clearly observed: there is sweep in the vegetation area (left region (y < 0.5) for Case 2, right region (y > 0.5) for Case 4) and ejection in the non-vegetation area (right region (y > 0.5) in Case 2, left region (y < 0.5) in Case 4), which elucidates the characteristics of the mixed layer and lateral exchange of mass and momentum.

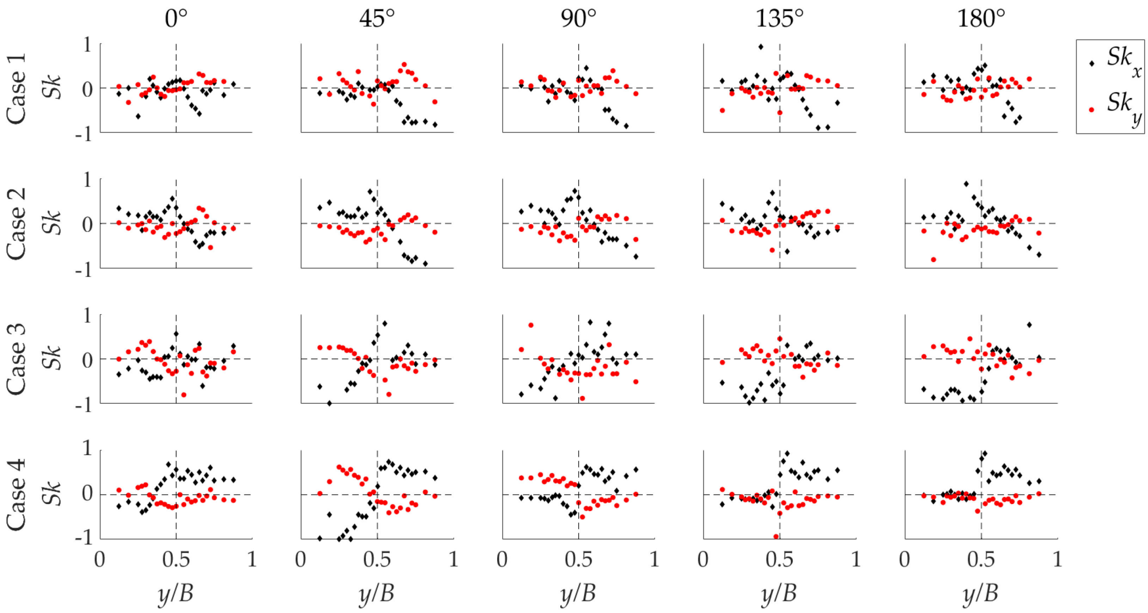

Figure 11. Lateral distribution of skewness coefficients of the longitudinal and lateral velocity fluctuating velocities from Case1 to Case 4.

Indeed, the lateral exchange of mass and momentum between the two areas of the channel was observed to decrease with decreasing vegetation density. For Cases 1 and 3 ($\phi = 2.235\%$), there is still $Sk_x < 0$ in non-vegetation area, but Sk_y has no evident trend like Cases 2 and 4. In general, the dominant turbulence event is apparent at the vegetation and non-vegetation interface for denser vegetation ($\phi = 4.47\%$) but not in sparser vegetation ($\phi = 2.235\%$).

4. Conclusions

Five experimental cases were conducted in a 180-degree U-shaped curved channel with different partly covered emerged vegetation. The transverse distribution of longitudinal velocity, turbulent kinetic energy, power spectral density and turbulent bursting affected by the emerged vegetation were analyzed in the experiments. The following main conclusions are given:

(1) For half-sided vegetation arrangement, the transverse distribution of the streamwise velocity along a curved channel presents a hyperbolic tangent function similar to that in a straight channel. There is a mixed layer with large flow velocity gradient at the interfacial area, which is not changed by the vegetation distributed along the convex or concave bank.

(2) When the vegetation is distributed along the concave bank, the response of streamwise velocity to the change of vegetation density is more significant. The velocity distribution in the vegetation areas and non-vegetation areas from the 0° to 90° sections reach a stable state near the wall, while it is not observed from the 135° to 180° sections.

(3) The combined impact of curved channel and vegetation increases the mixing between water bodies, resulting in the enhancement of turbulent kinetic energy. The influence of curve position on turbulence kinetic energy is far greater than that of vegetation density and vegetation distribution. The peak value of turbulent kinetic energy is comprehensively affected by vegetation density and distribution, and the peak position of turbulent kinetic energy at the interface is changed by different vegetation distribution.

(4) In the vegetation area, the amount of small-scale turbulence structure is minimal in comparison with the interface and non-vegetation areas. At the same time, the vortex dissipation rate in the bend increases and close to -1 through viscous friction, and the attenuation rate in the non-vegetation area is the largest, but at the interfacial area the attenuation rate is the smallest. Furthermore, the KH vortex in the mixing layer exists in the

curved channel, consistent with that in the straight channel, and the KH vortex frequency decreases with the development of the curve. It is obvious that the turbulence spectrum at the interface is affected by the vegetation density, and the peak frequency of the turbulence spectrum for denser vegetation is smaller, but there is no obvious correlation with the vegetation distribution.

(5) The frequency of occurrence for four types of turbulence events are affected by the curve and the partly covered vegetation. The inward and outward interactions are mainly bursting events in the vegetation area, while ejections and sweeps are dominant in the non-vegetation area, which are both affected by the location of the curve.

The results in this study can provide a scientific basis for flood control, water pollution control and river restoration. For example, planting emerged vegetation on the concave bank of a river can effectively reduce the flow rate at the concave bank and decrease bank scouring during floods, while the velocity and its distribution at different angles of the bend are also different. Due to the strongest turbulence events and material exchange at the vegetation and non-vegetation interface, we can control the range of pollutant diffusion by changing the density and location of vegetation in rivers. These flow field modifications not only influence the turbulent flow structure, but also change transport of sediments and nutrients in natural systems, with implications on a variety of biological and ecological processes.

This study has some shortcomings. For example, the measurement points were not dense enough, so the secondary circulation at different cross sections cannot be shown. Secondly, only two specific vegetation densities are set, and it was impossible to determine the critical vegetation density to initiate LSS along a curved channel. In addition, this study only carried out experiments when the flow rate was 30 L/s, and did not explore the effects of submerged vegetation, flexible vegetation and different flow conditions on the mixed layer structure. Therefore, hydraulic conditions such as discharge and water depth will be changed in future research, and the mixed layer will be studied in shallower flow cases. Furthermore, the ADV is unbale to measure the velocity near the water surface, so the other measurement techniques, such as particle image velocimetry (PIV), can be a good alternative. Finally, the *St* values (= 0.032) from s straight channel were adopted and possibly unsuitable for a curved channel. These aspects are worth comprehensive study in the future.

Author Contributions: Conceptualization: T.H., Y.L. and P.J.; methodology: T.H, Y.L. and K.H.; laboratory measurement: T.H. and M.H.; data analysis, T.H.; software, T.H. and M.H.; writing—original draft preparation, T.H. and Y.L.; writing—review and editing, K.H. and P.J.; funding acquisition, Y.L. and P.J. All authors have read and agreed to the published version of the manuscript.

Funding: This research was funded by the Key Research and Development Plan of China (2021YFE0206200), the Key-Area Research and Development Program of Guangdong Province (2021B07070030002), and the Science Foundation of Donghai Laboratory (Grant No. DH-2022KF01004, DH-2022KF01016). P.J. acknowledges the Startup Fund of the Hundred Talents Program at Zhejiang University, China.

Institutional Review Board Statement: Not applicable.

Informed Consent Statement: Not applicable.

Data Availability Statement: All data generated or analyzed during this study are included in this article.

Conflicts of Interest: The authors declare no conflict of interest.

References

1. Thomson, J. On the origin of windings of rivers in alluvial plains, with remarks on the flow of water round bends in pipes. *Proc. R. Soc. Lond.* **1876**, *25*, 5–8. [CrossRef]
2. Marion, A.; Zaramella, M. Effects of Velocity Gradients and Secondary Flow on the Dispersion of Solutes in a Meandering Channel. *J. Hydraul. Eng.* **2006**, *132*, 1295–1302. [CrossRef]

3. Blanckaert, K.; De Vriend, H.J. Secondary flow in sharp open-channel bends. *J. Fluid Mech.* **2004**, *498*, 353–380. [CrossRef]
4. Termini, D.; Piraino, M. Experimental analysis of cross-sectional flow motion in a large amplitude meandering bend. *Earth Surf. Process. Landf.* **2011**, *36*, 244–256. [CrossRef]
5. Rozovskii, I.L. *Flow of Water in Bends of Open Channels*; Israel Program for Scientific Translations: Jerusalem, Israel, 1961.
6. Booij, R. Measurements and large eddy simulations of the flows in some curved flumes. *J. Turbul.* **2003**, *4*, N8. [CrossRef]
7. Blanckaert, K.; Graf, W.H. Mean Flow and Turbulence in Open-Channel Bend. *J. Hydraul. Eng.* **2001**, *127*, 835–847. [CrossRef]
8. Zeng, J.; Constantinescu, G.; Blanckaert, K.; Weber, L. Flow and bathymetry in sharp open-channel bends: Experiments and predictions. *Water Resour. Res.* **2008**, *44*, W09401. [CrossRef]
9. Bodnár, T.; Příhoda, J. Numerical simulation of turbulent free-surface flow in curved channel. *Flow Turbul. Combust.* **2006**, *76*, 429–442. [CrossRef]
10. Naot, D.; Nezu, I.; Nakagawa, H. Hydrodynamic behavior of partly vegetated open channels. *J. Hydraul. Eng.* **1996**, *122*, 625–633. [CrossRef]
11. Kouwen, N.; Unny, T.E.; Hill, H.M. Flow retardance in vegetated channels. *J. Irrig. Drain. Div.* **1969**, *95*, 329–342. [CrossRef]
12. Nepf, H.M.; Vivoni, E.R. Flow structure in depth-limited, vegetated flow. *J. Geophys. Res. Ocean.* **2000**, *105*, 28547–28557. [CrossRef]
13. Lesieur, M.R. Mixing Layer Vortices. In *Fluid Vortices*; Springer: Dordrecht, The Netherlands, 1995; pp. 35–63. [CrossRef]
14. White, B.L.; Nepf, H.M. A vortex-based model of velocity and shear stress in a partially vegetated shallow channel. *Water Resour. Res.* **2008**, *44*, W01412. [CrossRef]
15. Ben Meftah, M.; Mossa, M. Partially obstructed channel: Contraction ratio effect on the flow hydrodynamic structure and prediction of the transversal mean velocity profile. *J. Hydrol.* **2016**, *542*, 87–100. [CrossRef]
16. Box, W.; Västilä, K.; Järvelä, J. Transport and deposition of fine sediment in a channel partly covered by flexible vegetation. *E3S Web Conf.* **2018**, *40*, 02016. [CrossRef]
17. Caroppi, G.; Gualtieri, P.; Fontana, N.; Giugni, M. Effects of vegetation density on shear layer in partly vegetated channels. *J. Hydro-Environ. Res.* **2020**, *30*, 82–90. [CrossRef]
18. Li, C.G.; Xue, W.Y.; Huai, W.X. Effect of vegetation on flow structure and dispersion in strongly curved channels. *J. Hydrodyn.* **2015**, *27*, 286–291. [CrossRef]
19. Gorrick, S.; Rodríguez, J.F. Flow and force-balance relations in a natural channel with bank vegetation. *J. Hydraul. Res.* **2014**, *52*, 794–810. [CrossRef]
20. Termini, D. Effect of Vegetation on Fluvial Erosion Processes: Experimental Analysis in a Laboratory Flume. *Procedia Environ. Sci.* **2013**, *19*, 904–911. [CrossRef]
21. Termini, D. Vegetation effects on cross-sectional flow in a large amplitude meandering bend. *J. Hydraul. Res.* **2017**, *55*, 423–429. [CrossRef]
22. Yang, Y.; Lin, Y.T.; Ji, X. Hydrodynamic characteristics of flow over emergent vegetation in a strongly curved channel. *J. Hydraul. Res.* **2022**, *60*, 240–257. [CrossRef]
23. Liu, C.; Shan, Y.; Liu, X.; Yang, K.; Liao, H. The effect of floodplain grass on the flow characteristics of meandering compound channels. *J. Hydrol.* **2016**, *542*, 1–17. [CrossRef]
24. Vaghefi, M.; Akbari, M.; Fiouz, A.R. An experimental study of mean and turbulent flow in a 180 degree sharp open channel bend: Secondary flow and bed shear stress. *KSCE J. Civ. Eng.* **2015**, *20*, 1582–1593. [CrossRef]
25. Goring, D.G.; Nikora, V.I. Despiking Acoustic Doppler Velocimeter Data. *J. Hydraul. Eng.* **2002**, *128*, 117–126. [CrossRef]
26. Kraus, N.C.; Lohrmann, A.; Cabrera, R. New Acoustic Meter for Measuring 3D Laboratory Flows. *J. Hydraul. Eng.* **1994**, *120*, 406–412. [CrossRef]
27. Nepf, H.M. Drag, turbulence, and diffusion in flow through emergent vegetation. *Water Resour. Res.* **1999**, *35*, 479–489. [CrossRef]
28. Ho, C.M.; Huerre, P. Perturbed free shear layers. *Annu. Rev. Fluid Mech.* **1984**, *16*, 365–424. [CrossRef]
29. Brown, G.L.; Roshko, A. On density effects and large structure in turbulent mixing layers. *J. Fluid Mech.* **2006**, *64*, 775–816. [CrossRef]
30. Chu, V.H.; Babarutsi, S. Confinement and Bed-Friction Effects in Shallow Turbulent Mixing Layers. *J. Hydraul. Eng.* **1988**, *114*, 1257–1274. [CrossRef]
31. Caroppi, G.; Västilä, K.; Järvelä, J.; Rowiński, P.M.; Giugni, M. Turbulence at water-vegetation interface in open channel flow: Experiments with natural-like plants. *Adv. Water Resour.* **2019**, *127*, 180–191. [CrossRef]
32. Dupuis, V.; Proust, S.; Berni, C.; Paquier, A. Mixing layer development in compound channel flows with submerged and emergent rigid vegetation over the floodplains. *Exp. Fluids* **2017**, *58*, 30. [CrossRef]
33. Balachandar, S. Turbulence, Coherent Structures, Dynamical Systems and Symmetry. *AIAA J.* **1998**, *36*, 496–496. [CrossRef]
34. Termini, D. Experimental analysis of the effect of vegetation on flow and bed shear stress distribution in high-curvature bends. *Geomorphology* **2016**, *274*, 1–10. [CrossRef]
35. Welch, P. The use of fast Fourier transform for the estimation of power spectra: A method based on time averaging over short, modified periodograms. *IEEE Trans. Audio Electroacoust.* **1967**, *15*, 70–73. [CrossRef]
36. Huai, W.X.; Zhang, J.; Wang, W.J.; Katul, G.G. Turbulence structure in open channel flow with partially covered artificial emergent vegetation. *J. Hydrol.* **2019**, *573*, 180–193. [CrossRef]

37. Ghisalberti, M.; Nepf, H.M. Mixing layers and coherent structures in vegetated aquatic flows. *J. Geophys. Res. Ocean.* **2002**, *107*, 3-1–3-11. [CrossRef]
38. Ghisalberti, M.; Nepf, H. The Structure of the Shear Layer in Flows over Rigid and Flexible Canopies. *Environ. Fluid Mech.* **2006**, *6*, 277–301. [CrossRef]
39. Lu, S.S.; Willmarth, W.W. Measurements of the structure of the Reynolds stress in a turbulent boundary layer. *J. Fluid Mech.* **2006**, *60*, 481–511. [CrossRef]
40. Duan, J.; He, L.; Wang, G.; Fu, X. Turbulent burst around experimental spur dike. *Int. J. Sediment Res.* **2011**, *26*, 471–523. [CrossRef]
41. Mohajeri, S.H.; Righetti, M.; Wharton, G.; Romano, G.P. On the structure of turbulent gravel bed flow: Implications for sediment transport. *Adv. Water Resour.* **2016**, *92*, 90–104. [CrossRef]
42. Afzalimehr, H.; Moghbel, R.; Gallichand, J.; Sui, J. Investigation of turbulence characteristics in channel with dense vegetation. *Int. J. Sediment Res.* **2011**, *26*, 269–282. [CrossRef]
43. Zhao, H.; Yan, J.; Yuan, S.; Liu, J.; Zheng, J. Effects of Submerged Vegetation Density on Turbulent Flow Characteristics in an Open Channel. *Water* **2019**, *11*, 2154. [CrossRef]